WALL-MODELED LES OF BUFFET UNDER THE INFLUENCE OF ENGINE NACELLE FLOW

T. Lürkens*, M. Meinke*,†, W. Schröder*,†

* RWTH Aachen University, Chair of Fluid Mechanics and Institute of Aerodynamics, Wüllnerstraße 5a, 52062 Aachen

† RWTH Aachen University, JARA Center for Simulation and Data Science, Seffenter Weg 23, 52074 Aachen

Abstract

A wall-modeled large-eddy simulation of the OAT15A airfoil complemented by a nacelle of a generic ultra-high bypass ratio turbofan engine is performed at Mach number $Ma = 0.73$, angle of attack $\alpha = 3.5°$, and chord based Reynolds number $Re_c = 2 \cdot 10^6$. The presence of the nacelle geometry leads to noticeable changes of the flow conditions of the airfoil which are characterized by streamline diversion and a shock wave on the upper part of the nacelle. The dynamics of the shock waves is analyzed using dynamic mode decomposition revealing shared fundamental frequencies, which can be reconciled with established buffet models.

Keywords

Shock Buffet; Engine Nacelle Flow; Wall-Modeled LES

NOMENCLATURE

Symbols

α	angle of attack
c	chord length
c_p	pressure coefficient
κ	von Karman's constant
$\boldsymbol{L}$	Lamb vector
Ma	Mach number
μ	dynamic viscosity
Re	Reynolds number
ρ	density
Sr	Strouhal number
τ	shear stress
$\boldsymbol{u}$	velocity vector

Indices

$'$	perturbed quantity
∞	freestream
nac	related to the nacelle
oat	related to the airfoil
$\|\|$	wall-parallel
$+$	inner units
w	at the wall
wm	wall-model

Abbreviations

CTU	Convective time unit
DMD	Dynamic mode decomposition
FFT	Fast Fourier transform
LES	Large-eddy simulation
UHBR	Ultra-high bypass ratio
WM-LES	Wall-modeled large-eddy simulation
WR-LES	Wall-resolved large-eddy simulation

1. INTRODUCTION

Transonic flow around supercritical airfoils is characterized by a supersonic region on the airfoil suction side terminated by a shock wave. For certain combinations of angle of attack and freestream Mach number the shock wave is subject to self-sustained low-frequency oscillations referred to as buffet. The structural response of the wing to these shock oscillations, which is denoted buffeting, poses a risk for the integrity of the structure, and consequently, the buffet boundary represents a strict limit to the flight envelope. Proper prediction of the aeroelastic behavior is crucial in the economically and ecologically driven endeavor to design lighter and more

doi: 10.25967/570433

fuel efficient aircraft. Therefore, a thorough understanding of the buffet phenomenon is substantially important in the design process of future aircraft.
The most established model explaining the self-sustained nature of the low-frequency shock oscillation has been introduced by Lee [1]. This model is based on considering a closed feedback loop between the shock induced separation on the airfoil suction side and the acoustics generated in the vicinity of the trailing edge. Vortices are caused by the shock-wave/boundary-layer interaction traveling downstream. When passing over the trailing edge, the vortices generate pressure waves by the transition from a wall-bounded to a free-shear layer that propagate back upstream and interact with the shock pushing it upstream. Having reached the most upstream position, the massive shock induced separation leads to a reduction of the sound pressure level at the trailing edge such that the shock moves downstream which closes the feedback loop. Good agreement with Lee's theory was found by Xiao et al. [2], Deck [3], Hartmann et al. [4–6] and Feldhusen-Hoffmann et al. [7,8]. A modification to Lee's model was proposed by Hartmann et al. [6] stating that the relevant interaction region between the shock and pressure waves is not at the shock foot but at its upper end. Thereby, the agreement between the measured buffet frequency and the buffet frequency predicted by the model could be improved significantly.
Jet engines mounted closely underneath the wing have a significant effect on the overall flow field. The shear layer that develops on the upper part of the engine nacelle impacts the boundary layer on the airfoil pressure side leading to an altered trailing edge flow. The trailing edge flow, however, is a significant element of established buffet models [1, 6] such that the shock oscillation can be strongly influenced.
Furthermore, in transonic flow unsteady shock waves occur on the engine nacelle [9,10]. The presence of a shock wave upstream of the airfoil dramatically alters the flow to the airfoil. Due to the sensitivity of the buffet phenomenon to the upstream flow conditions the shock buffet also changes. The novel flow conditions to the airfoil directly affect the quality of the shock buffet.
While transonic shock buffet has been studied extensively in the recent years [1–8, 11, 12], little is known about the interaction of engine induced flow disturbances and the involved dynamics. Yet, engine nacelle integration is an important aspect of the aerodynamic design of commercial aircraft. This means, it is of great interest to complement the current knowledge by the effect of engine induced flow disturbances on the buffet phenomenon.
In this study, the flow field around the OAT15A airfoil including a generic 2D-periodic ultra-high bypass ratio (UHBR) engine nacelle at buffet conditions is computed using wall-modeled large-eddy simulations (WM-LES). The flow field is analyzed with focus on the dynamics in comparison with comparable setups from literature. The paper is organized as follows. In section 2, the simulation framework is briefly introduced. The wall-modeling approach is discussed and the dynamic mode decomposition (DMD) is briefly introduced. In section 3, the computational setup is presented. The results are discussed in section 4 with subsection 4.1 dealing in detail with the dynamics on the nacelle, whereas subsection 4.2 focuses on the dynamics on the airfoil. In subsection 4.3, the wake flow of the nacelle is considered. Concluding remarks are given in section 5.

2. NUMERICAL METHODS

All simulations are performed using the Cartesian finite-volume solver of the m-AIA framework which was formerly denoted ZFS [13]. The underlying governing equations are the compressible, unsteady Navier-Stokes equations. The equations are spatially filtered and solved on an unstructured, hierarchical Cartesian mesh using the finite-volume method. The advective upstream splitting method (AUSM) is used for the convective fluxes. A central difference scheme is employed for the discretization of the viscous fluxes. For the temporal integration, a second-order accurate 5-stage Runge-Kutta method is used. Small scale turbulence is accounted for by the approach of monotonically integrated LES (MILES) [14] such that no additional turbulence model is necessary [15]. Boundaries of embedded bodies are realized using a Cartesian cut-cell method [16]. More details of the m-AIA simulation framework are given in [15, 16].

2.1. Wall-stress model

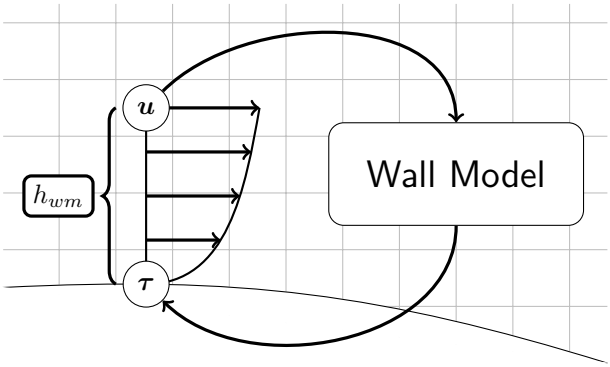

FIG 1. Graphic representation of the wall-model mechanism.

Wall-modeling approaches are a convenient method to circumvent the massive constraints on mesh resolution for conventional LES of boundary layer flows while maintaining a high spatial and temporal resolution. Omitting the resolution of the viscous sublayer and only resolving large scale structures scaling with the outer units WM-LES enables not only a significant reduction in the total number of cells but at the same time allows a substantially larger time step. Thereby, LES of dynamic phenomena at low Strouhal numbers $Sr = \frac{f \cdot c}{u_\infty}$ can be performed even for high Reynolds numbers within a reasonable time frame. The applicability of the method to buffet flows has been demonstrated by Fukushima & Kawai [17].
In this study, an analytical wall-stress model is used to compute the wall-shear stress based on flow information obtained from the outer boundary layer. The function

used is an implicit single equation expression for the law of the wall introduced by Spalding [18]:

$$y^+ = u^+ + e^{-\kappa B}\left\{e^{\kappa u^+} - \sum_{n=0}^{4}\frac{(\kappa u^+)^n}{n!}\right\} \tag{1}$$

with $u^+ = \frac{u_\parallel}{u_\tau}$, $y^+ = \frac{h_{wm}u_\tau}{\nu}$ and $u_\tau = \sqrt{\tau_w/\rho_w}$. The subscript $(\bullet)_\parallel$ denotes projection on the wall-tangential plane. The von Kármán constant κ is set to 0.4 and B is set to 5.0. Equation 1 is evaluated at a sampling distance $y = h_{wm}$ normal to the surface which is illustrated in figure 1. The implicit expression is then solved iteratively for u_τ using Newton's method. To apply the computed wall-shear stress to the boundary surface an additional correction loop within the viscous flux computation is performed adding an artificial viscosity μ_{wm} such that the condition

$$(\mu + \mu_{wm})\frac{\partial u_\parallel}{\partial n} = \tau_{wm} \tag{2}$$

is satisfied. To prevent an obvious misapplication of the model in regions of separated flow the velocity gradient at the wall is checked for $\partial u_\parallel/\partial n < 0$. If flow separation is detected, the application of the wall-model is omitted by setting $\mu_{wm} = 0$.

2.2. Dynamic mode decomposition

The dynamic mode decomposition (DMD) [19] is a data-driven technique that allows the decomposition of a given data field $\boldsymbol{q}(\boldsymbol{x}, t)$ into a series representation of spatio-temporal modes ϕ_n. Every mode is characterized by an individual, complex frequency λ_n, and amplitude a_n. The resulting series representation of the data field reads

$$\boldsymbol{q}(\boldsymbol{x}, t) = \sum_n a_n e^{\lambda_n t}\boldsymbol{\phi}_n(\boldsymbol{x}). \tag{3}$$

When these modes are determined characteristic dynamic phenomena of distinct frequencies can be isolated and studied in detail. The buffet phenomenon is typically restricted to narrow frequency bands such that DMD can be an effective tool for the in-depth analysis of the isolated dynamics and the underlying physical mechanisms. In the recent past, DMD has been successfully applied to both experimental and numerical flow field data of buffet flows [8, 20–23]. All DMD analyses have been performed using the flowTorch library developed by Weiner & Semaan [24].

3. COMPUTATIONAL SETUP

Computing the wall-shear stress from the wall model discussed in section 2.1 requires a fully attached boundary layer flow. However, buffet flows at high angles of attack can be subject to massive flow separation due to the shock-wave/boundary-layer interaction. Therefore, a setup with only mild flow separation while still providing low-frequency shock oscillations is considered. Based on the work by Fukushima & Kawai [17], Jacquin et al. [12] and Deck [3] the angle of attack was set to $\alpha = 3.5°$

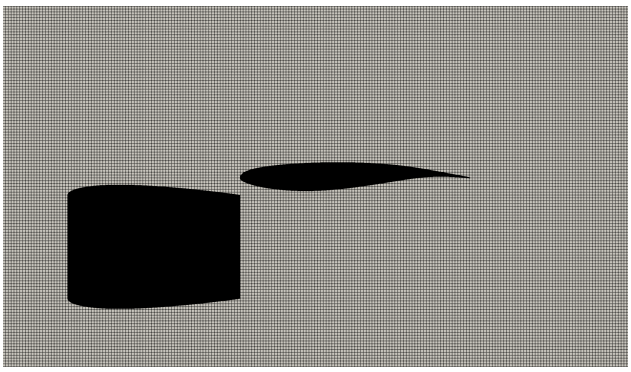

FIG 2. Computational mesh on the coarsest level.

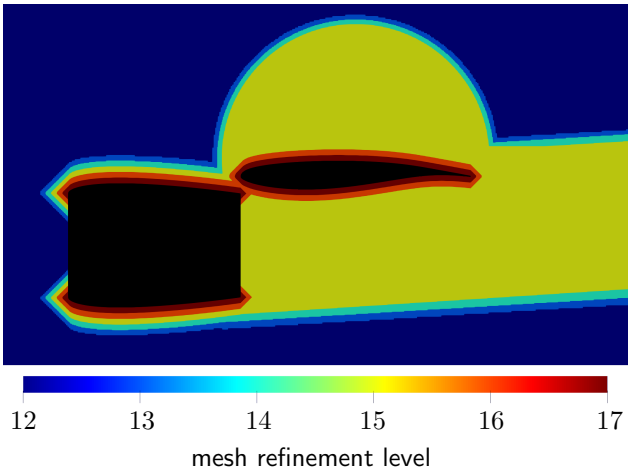

FIG 3. Regions of grid refinement around the OAT15A and the nacelle geometry.

and the freestream Mach number to $Ma_\infty = 0.73$. In agreement with the associated experimental study by Schauerte & Schreyer [25] the chord based Reynolds number was set to $Re_c = 2 \cdot 10^6$.

For the nacelle, a generic geometry based on a NACA 0012 airfoil was generated. The outer dimensioning of the nacelle geometry with respect to the local chord length is roughly based on the UHBR flow-through nacelle by Spinner & Rudnik [10], which was designed for the Airbus XRF1 research model. That is, the inlet and outlet diameter was set to $d_{nac} = 0.45c$ and the nacelle length to $l_{nac} = 0.75c$.

The grid dimensions are given by $L_x \times L_y \times L_z = 25.4c \times 24.9c \times 0.05c$, which proved to be sufficient for comparable flows by Zauner & Sandham [26] and Moise et al. [27]. The grid is locally refined within the boundary layer satisfying the mesh requirements for WM-LES proposed by Kawai & Larsson [28]. That is, at least 20 cells are located within the boundary layer at $x_{oat}/c = 0.2$ and $x_{nac}/c = 0.2$. Since the acoustics in the vicinity of the trailing edge is a key element of established buffet models additional a-priori refinement is applied on the suction side of the airfoil and in the wake region of the airfoil and the nacelle. This results in a total mesh size of about $1.24 \cdot 10^9$ cells. The Cartesian mesh on the coarsest refinement level is shown in figure 2. Regions of additional mesh refinement are highlighted by a color distribution in figure 3. The wall model is applied to

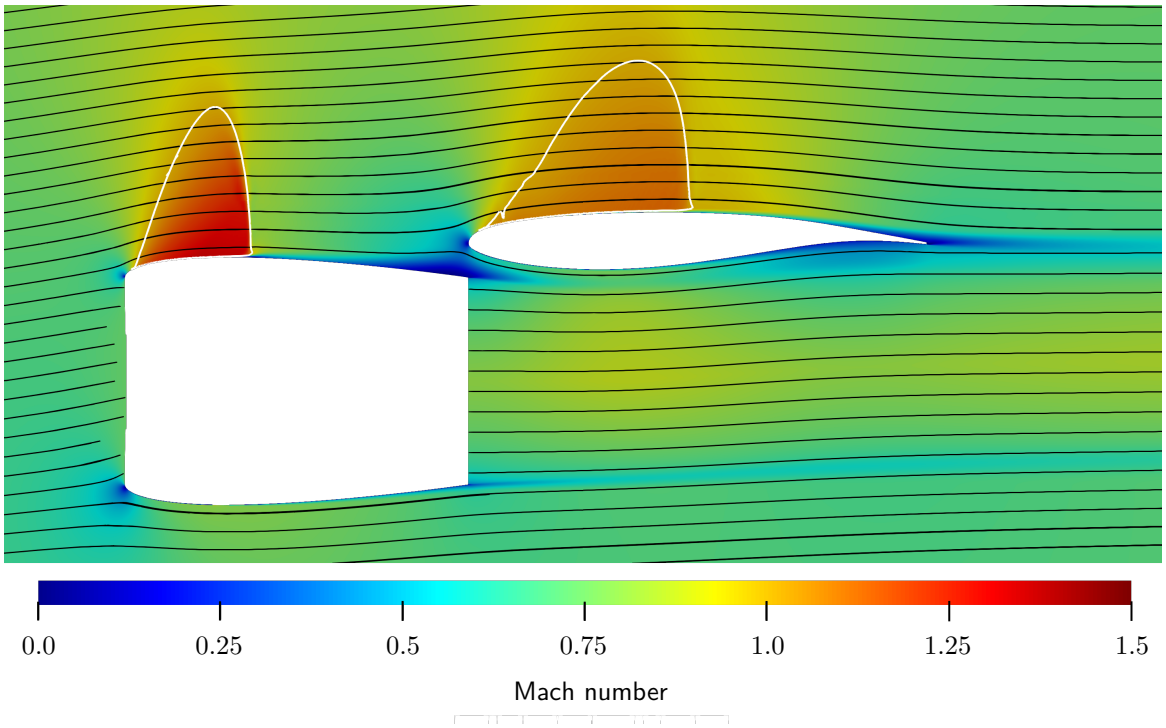

FIG 4. Mach number contours of the mean flow field, white lines indicate sonic lines ($Ma = 1$), black lines denote streamlines.

all solid wall boundaries. The evaluation distance h_{wm} of the wall model is set to a distance of approximately three cell lengths from the wall, satisfying the requirements proposed by Kawai & Larsson [28]. A characteristic outflow boundary condition is used for the main outflow plane to suppress spurious reflections. Standard in- and outflow boundary conditions with sponge layers are applied to the remaining in- and outflow planes in the x- and y-direction. Periodicity is applied to spanwise boundaries. Obviously, this is a great simplification of the in general highly three-dimensional flow field around the engine nacelle. This, however, allows to study the effect of the upstream shock wave and the free-shear layer introduced by the nacelle geometry onto the buffet phenomenon while keeping the total number of grid points at a manageable level. On the nacelle inlet, a standard outflow boundary condition is applied. For the engine outlet, a $1/7$th power law velocity profile is prescribed while maintaining mass conservation with the engine inlet. Hence, the setup represents a simple flow-through nacelle.

To enforce a controlled transition of the boundary layer into a turbulent state the tripping method by Schlatter and Örlu [29] is employed at $x/c = 0.07$ on both sides of the airfoil.

4. RESULTS

To analyze the flow field data, samples were collected for a total of 70 convective time units defined as $CTU = c/u_\infty$. Spanwise averaged probes on the nacelle and airfoil surface were taken every 1% of the chord length with a sampling interval of $4.1 \cdot 10^{-3}\, CTU$. To analyze the occurring dynamics using dynamic mode decomposition, data samples in the xy-plane at $z = 0.025$ of the global flow field were taken at a sampling step of $0.0986\, CTU$.

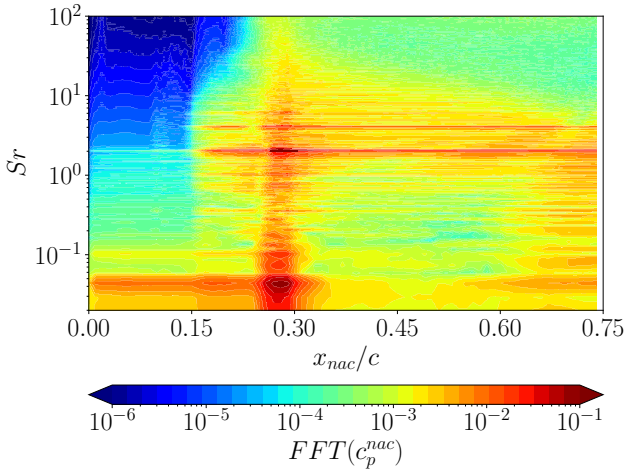

FIG 5. Streamwise distibution of the frequency spectrum of the pressure signal on the nacelle.

In figure 4, Mach number contours of the mean flow field with overlayed streamlines are shown. The acceleration of the flow on the upper part of the engine nacelle is terminated by a prominent recompression shock. The streamline diversion due to the flow following the contour of the nacelle indicates that the effective angle of attack of the airfoil is reduced compared to an undisturbed inflow at $\alpha = 3.5°$. Additionally, the boundary layer that forms along the top of the nacelle leads to a pronounced velocity deficit in the flow field over the pressure side of the airfoil. This multitude of disturbances introduced by the engine nacelle into the flow field implies drastic

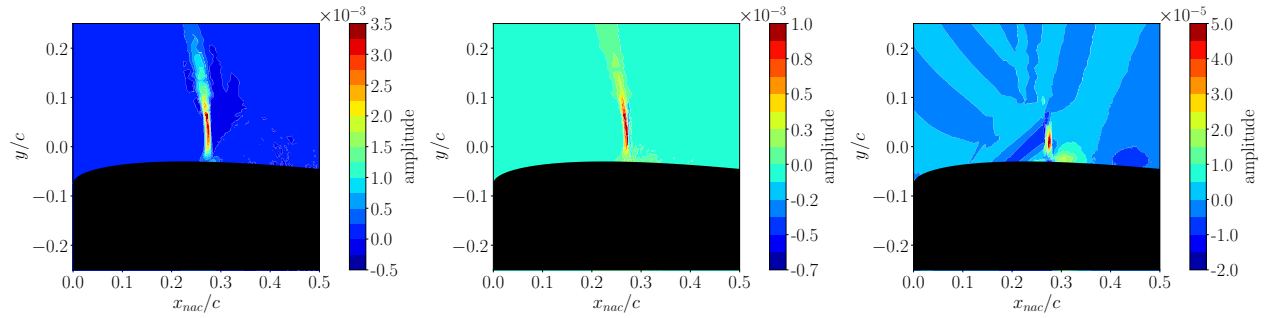

(a) $Sr = 0.036$ **(b)** $Sr = 0.072$ **(c)** $Sr = 2.00$

FIG 6. Real part of pressure modes on the upper side of the nacelle extracted by DMD.

changes to the flow conditions of the airfoil, the effects of which on the buffet phenomenon will be discussed in the following sections.

4.1. Nacelle

Before starting with the analysis of the flow around the OAT15A airfoil, a closer look is taken at the flow details around the nacelle. On the upper side of the nacelle, a strong recompression shock was already identified in the mean flow field. In figure 5, the streamwise distribution of the frequency spectrum of the surface pressure signal on the upper side of the nacelle is shown revealing multiple dynamic features. In the region of the shock from $0.25c < x_{nac} < 0.31c$ a low-frequency peak occurs, which lies in the characteristic range of transonic shock buffet. Additionally, a sharp high-frequency peak at $Sr = 2.0$ and the corresponding upper harmonics are prominent starting upstream of the shock at $x_{nac} = 0.15c$. From their origin, these high-frequency peaks propagate downstream and persist to the trailing edge. To extract the isolated dynamics at these frequencies, dynamic mode decomposition of the flow field data was performed. In figure 6a, the low-frequency mode of the pressure field at $Sr = 0.036$ is shown. In correspondence with the the upper harmonic mode at $Sr = 0.072$ in figure 6b this frequency can be associated with a low-frequency oscillation of the shock which possesses, however, a rather small amplitude. The high-frequency mode at $Sr = 2.00$ is shown in figure 6c. It corresponds to the interaction of the incoming boundary layer with the shock wave and the associated transition from laminar to turbulent flow.

4.2. OAT15A

Figure 7 shows the mean pressure coefficient and the instantaneous pressure coefficient at the most upstream and the most downstream shock position. It is evident that the pressure minimum upstream of the shock wave is attenuated significantly from the pressure plateau known from literature for the given flow conditions without the nacelle [3, 12]. This can be associated with the reduced effective angle of attack and the lower kinetic energy in the incoming flow. Both effects are, however, hard to quantify without detailed reference data. Altogether, this leads to a considerably weaker shock on the airfoil suction

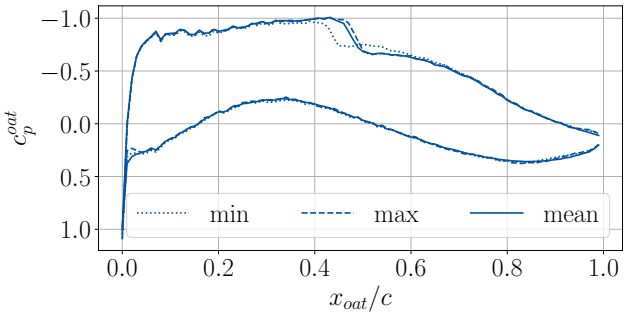

FIG 7. Mean pressure coefficient on the OAT15A airfoil and instantaneous pressure coefficient at upstream and downstream shock position.

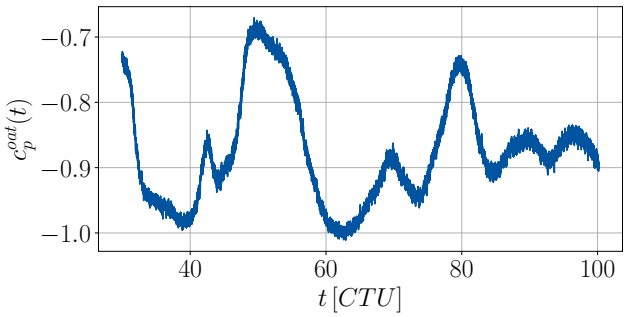

FIG 8. Pressure signal at the mean shock position $x_{oat} = 0.47$.

side around $x_{oat}/c = 0.47$. Looking at the extrema of the shock position, it is noticeable that the mean shock position is clearly closer to the most downstream position than to the most upstream position, indicating rather uneven shock dynamics. In figure 10, the streamwise distribution of the frequency spectrum of the surface pressure signal is shown. The spectrum is clearly dominated by a low-frequency peak in the shock region with a frequency of $Sr = 0.036$. This is significantly lower than the buffet frequency of $Sr = 0.065$ found by Deck [3], Jacquin et al. [12], and Fukushima & Kawai [17] at the higher Reynolds number of $Re_c = 3 \cdot 10^6$. Note, however, that no engine was considered in [3, 12, 17]. In figure 8, the signal of the surface pressure at $x_{oat} = 0.47$, which corresponds to the mean shock position is given. The signal clearly exhibits large-amplitude low-frequency dynamics. However, the signal shows a much more chaotic behavior compared to undisturbed buffet cases, whose local pres-

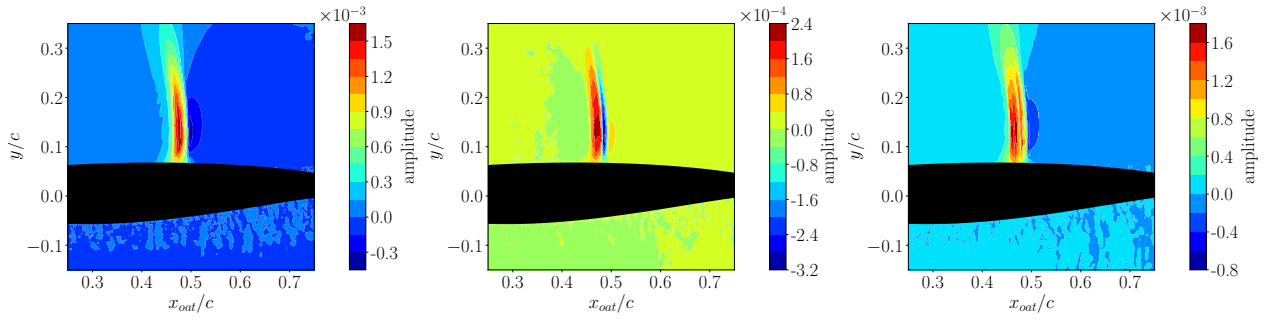

(a) $Sr = 0.036$ **(b)** $Sr = 0.072$ **(c)** $Sr = 0.108$

FIG 9. Real part of pressure modes on the OAT15A airfoil extracted by DMD.

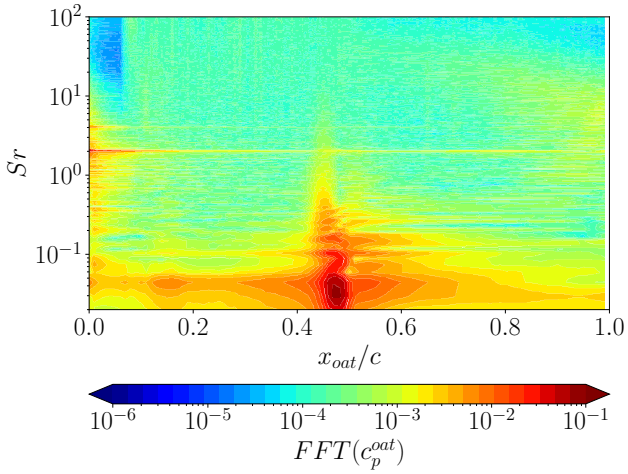

FIG 10. Streamwise distribution of the frequency spectrum of the pressure signal on the OAT15A.

sure signals in the shock region resemble a much more harmonic signal [12]. From the time signal it is reasonable that the lower fundamental frequency obtained from the FFT of the pressure signal can be related to the large amplitude variations within the pressure signal. The general dynamics, however, appears to take place at a higher harmonic. This hypothesis is supported by the pressure modes given in figure 9. The spatial extent of the mode at a frequency of $Sr = 0.108$ exceeds that of the fundamental frequency of $Sr = 0.036$ and its upper harmonic at $Sr = 0.072$ and exhibits a comparable or even larger amplitude in the shock region. It is, however, remarkable that the shock on the nacelle and the shock on the airfoil share a fundamental frequency at $Sr = 0.036$. Compared to the shock dynamics found in the literature [3, 12, 17], the quality of the buffet in this study exhibits rather irregular behavior and is of significantly lower amplitude. Considering the reduction of the effective angle of attack by the nacelle geometry, it is reasonable that the buffet is shifted from developed buffet into the regime of buffet onset.

It is noteworthy that the high-frequency peak at $Sr = 2.0$ originating from the oscillation of the shock foot on the nacelle is also found on the OAT15A. The signal, however, dissipates rather quickly as it propagates downstream. Figure 10 shows that in the shock region no re-amplification of the high-frequency peak can be found, indicating that the shock dynamics remains unaffected by the incoming high-frequency disturbance.

4.3. Wake flow

Established buffet models link the low-frequency shock oscillation to the acoustics generated by the shear flow in the vicinity of the trailing edge [1, 6]. From the mean flow field shown in figure 4, it is evident that the wake of the upper part of the nacelle interferes with the boundary layer on the airfoil pressure side such that also the trailing edge flow is affected. The velocity component in the main flow direction was analyzed by DMD to investigate the dynamics of the boundary layer. The extracted mode at the fundamental frequency $Sr = 0.036$ shared by the shock on the nacelle and that on the suction side of the airfoil is given in figure 11. An inverse dynamics of periodic acceleration and deceleration of the boundary layer between the suction and the pressure side of the airfoil is observed at this very frequency. The dynamics on the pressure side appears to be driven by the wake flow emerging from the upper part of the nacelle which subsequently interacts with the boundary layer. The alternating behavior of the suction and pressure side boundary layer leads to a periodic increase and decrease of the shear rate in the vicinity of the trailing edge. The shear rate fluctuation, however, is part of the dominating acoustic source term in shear flows, i.e., the perturbed Lamb vector [30], which is given by the curl of the velocity vector and the vorticity vector

$$\boldsymbol{L}' = (\boldsymbol{u} \times (\nabla \times \boldsymbol{u}))' . \tag{4}$$

Consequently, we can associate the shared fundamental frequency at $Sr = 0.036$ with the acoustics created by the shear flow at the trailing edge. Accordingly, the shared dynamics of the two compression shocks can be explained within the framework of existing buffet models. To confirm this hypothesis, however, more detailed investigations of the acoustics in the vicinity of the trailing edge are necessary.

5. CONCLUSION & OUTLOOK

A wall-modeled LES of the OAT15A airfoil including a generic flow-through UHBR engine nacelle has been performed at buffet conditions. The presence of the nacelle

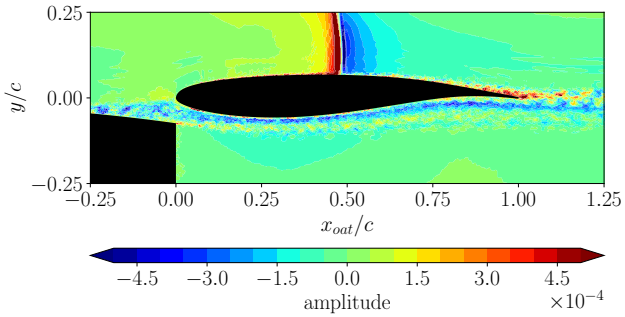

FIG 11. Real part of the streamwise velocity mode at $Sr = 0.036$ extracted by DMD.

has a strong influence on the overall flow field. The diversion of the streamlines due to the nacelle geometry reduces the effective angle of attack of the airfoil. Additionally, the kinetic energy of the flow to the airfoil is reduced by a strong compression shock on the upper side of the nacelle. To analyze the shock dynamics, dynamic mode decomposition was performed on the flow field data. Shared fundamental frequencies are identified in the dynamics of the shock on the nacelle and on the airfoil, which can be explained within the framework of established buffet models. However, detailed investigation of the actual acoustics in the vicinity of the trailing edge is necessary to consolidate this hypothesis. Compared to the developed buffet known from literature at the given flow conditions, the dynamics of the shock buffet on the airfoil exhibit a highly irregular behavior, suggesting the flow disturbance by the engine nacelle shifts the buffet into the regime of buffet onset. High-frequency pressure waves originating from the shock on the upper side of the engine nacelle propagate over the suction side of the airfoil. However, no interaction with the dynamics of the shock wave on the airfoil could be observed.
The reduction of the engine nacelle to a 2D-periodic solid body with dedicated inflow and outflow boundaries allowed a controlled study of the effect of the altered flow conditions of the airfoil at reasonable costs. Yet, these simplifications raise the question of how a properly resolved three-dimensional engine featuring accelerated core and bypass flows affects these results. This will be computed and analyzed in future studies.

Acknowledgements

The authors gratefully acknowledge the Gauss Centre for Supercomputing e.V. (www.gauss-centre.eu) for funding this project by providing computing time on the GCS Supercomputer HAWK at Höchstleistungsrechenzentrum Stuttgart (www.hlrs.de).

The authors gratefully acknowledge the Deutsche Forschungsgemeinschaft DFG (German Research Foundation) for funding this work in the framework of the research unit FOR 2895 (project number 406435057).

The authors wish to thank Dr.-Ing. Andre Weiner and Dr. Richard Semaan for the development of the flowTorch library.

The authors also wish to thank ONERA for providing the OAT15A airfoil geometry.

Contact address:

t.luerkens@aia.rwth-aachen.de

References

[1] B. H. K. Lee. Self-sustained shock oscillations on airfoils at transonic speeds. *Progress in Aerospace Sciences*, 37(2):147–196, 2001. DOI: 10.1016/S0376-0421(01)00003-3.

[2] Q. Xiao, H. M. Tsai, and F. Liu. Numerical study of transonic buffet on a supercritical airfoil. *AIAA Journal*, 44(3):620–628, 2006. DOI: 10.2514/1.16658.

[3] S. Deck. Numerical simulation of transonic buffet over a supercritical airfoil. *AIAA Journal*, 43(7):1556–1566, 2005. DOI: 10.2514/1.9885.

[4] A. Hartmann, M. Klaas, and W. Schröder. Time-resolved stereo PIV measurements of shock–boundary layer interaction on a supercritical airfoil. *Experiments in Fluids*, 52(3):591–604, 2012. DOI: 10.1007/s00348-011-1074-6.

[5] A. Hartmann, M. Klaas, and W. Schröder. Coupled airfoil heave/pitch oscillations at buffet flow. *AIAA Journal*, 51:1542–1552, 06 2013. DOI: 10.2514/1.J051512.

[6] A. Hartmann, A. Feldhusen, and W. Schröder. On the interaction of shock waves and sound waves in transonic buffet flow. *Physics of Fluids*, 25(2):026101, 2013. DOI: 10.1063/1.4791603.

[7] A. Feldhusen-Hoffmann, V. Statnikov, M. Klaas, and W. Schröder. Investigation of shock–acoustic-wave interaction in transonic flow. *Experiments in Fluids*, 59:15, 12 2017. DOI: 10.1007/s00348-017-2466-z.

[8] A. Feldhusen-Hoffmann, C. Lagemann, S. Loosen, P. Meysonnat, M. Klaas, and W. Schröder. Analysis of transonic buffet using dynamic mode decomposition. *Experiments in Fluids*, 62:66, 04 2021. DOI: 10.1007/s00348-020-03111-5.

[9] G. Dietz, H. Mai, A. Schröder, C. Klein, N. Moreaux, and P. Leconte. Unsteady wing-pylon-nacelle interference in transonic flow. *Journal of Aircraft*, Vol. 45:934–944, 01 2008. DOI: 10.2514/6.2007-2018.

[10] S. Spinner and R. Rudnik. Design of a uhbr through flow nacelle for high speed stall wind tunnel investigations. In *Deutscher Luft- und Raumfahrtkongress 2021*. Deutsche Gesellschaft für Luft- und Raumfahrt - Lilienthal-Oberth e.V., 2021.

[11] N. F. Giannelis, G. A. Vio, and O. Levinski. A review of recent developments in the understanding of transonic shock buffet. *Progress in Aerospace Sciences*, 92:39–84, 2017. ISSN: 0376-0421. DOI: 10.1016/j.paerosci.2017.05.004.

[12] L. Jacquin, P. Molton, S. Deck, B. Maury, and D. Soulevant. Experimental study of shock oscillation over a transonic supercritical profile. *AIAA Journal*, 47(9):1985–1994, 2009. DOI: 10.2514/1.30190.

[13] A. Lintermann, M. Meinke, and W. Schröder. Zonal flow solver (ZFS): a highly efficient multi-physics simulation framework. *International Journal of Computational Fluid Dynamics*, 34(7-8):458–485, 2020. DOI: 10.1080/10618562.2020.1742328.

[14] J. P. Boris, F. F. Grinstein, E. S. Oran, and R. L. Kolbe. New insights into large eddy simulation. *Fluid Dynamics Research*, 10(4-6):199–228, 12 1992. DOI: 10.1016/0169-5983(92)90023-p.

[15] M. Meinke, W. Schröder, E. Krause, and Th. Rister. A comparison of second- and sixth-order methods for large-eddy simulations. *Computers & Fluids*, 31(4):695–718, 2002. DOI: 10.1016/S0045-7930(01)00073-1.

[16] L. Schneiders, C. Günther, M. Meinke, and W. Schröder. An efficient conservative cut-cell method for rigid bodies interacting with viscous compressible flows. *Journal of Computational Physics*, 311:62–86, 2016. ISSN: 0021-9991. DOI: 10.1016/j.jcp.2016.01.026.

[17] Y. Fukushima and S. Kawai. Wall-modeled large-eddy simulation of transonic airfoil buffet at high reynolds number. *AIAA Journal*, 56(6):2372–2388, 2018. DOI: 10.2514/1.J056537.

[18] D. B. Spalding. A Single Formula for the "Law of the Wall". *Journal of Applied Mechanics*, 28(3):455–458, 09 1961. DOI: 10.1115/1.3641728.

[19] P. J. Schmid. Dynamic mode decomposition of numerical and experimental data. *Journal of Fluid Mechanics*, 656:5–28, 2010. DOI: 10.1017/S0022112010001217.

[20] J. Kou and W. Zhang. An improved criterion to select dominant modes from dynamic mode decomposition. *European Journal of Mechanics - B/Fluids*, 62:109–129, 2017. ISSN: 0997-7546. DOI: 10.1016/j.euromechflu.2016.11.015.

[21] J. Kou, S. Le Clainche, and W. Zhang. A reduced-order model for compressible flows with buffeting condition using higher order dynamic mode decomposition with a mode selection criterion. *Physics of Fluids*, 30(1):016103, 2018. DOI: 10.1063/1.4999699.

[22] C. Gao, W. Zhang, J. Kou, Y. Liu, and Z. Ye. Active control of transonic buffet flow. *Journal of Fluid Mechanics*, 824:312–351, 2017. DOI: 10.1017/jfm.2017.344.

[23] L. Poplingher, D. E. Raveh, and E. H. Dowell. Modal analysis of transonic shock buffet on 2d airfoil. *AIAA Journal*, 57(7):2851–2866, 2019. DOI: 10.2514/1.J057893.

[24] A. Weiner and R. Semaan. flowtorch - a python library for analysis and reduced-order modeling of fluid flows. *Journal of Open Source Software*, 6(68):3860, 2021. DOI: 10.21105/joss.03860.

[25] C. J. Schauerte and A.-M. Schreyer. Experimental analysis of transonic buffet conditions on a two-dimensional supercritical airfoil (under review). *AIAA Journal*, 2022.

[26] M. Zauner and N. D. Sandham. Wide domain simulations of flow over an unswept laminar wing section undergoing transonic buffet. *Physical Review Fluids*, 5:083903, Aug 2020. DOI: 10.1103/PhysRevFluids.5.083903.

[27] P. Moise, M. Zauner, and N. D. Sandham. Large eddy simulations and modal reconstruction of laminar transonic buffet (under revision). *Journal of Fluid Mechanics*, 2021.

[28] S. Kawai and J. Larsson. Wall-modeling in large eddy simulation: Length scales, grid resolution, and accuracy. *Physics of Fluids*, 24(1):015105, 2012. DOI: 10.1063/1.3678331.

[29] P. Schlatter and R. Örlü. Turbulent boundary layers at moderate reynolds numbers: inflow length and tripping effects. *Journal of Fluid Mechanics*, 710:5–34, 2012. DOI: 10.1017/jfm.2012.324.

[30] R. Ewert and W. Schröder. Acoustic perturbation equations based on flow decomposition via source filtering. *Journal of Computational Physics*, 188(2):365–398, 2003. DOI: 10.1016/S0021-9991(03)00168-2.